Tts1, the fission yeast homologue of the TMEM33 family, functions in NE remodeling during mitosis

Dan Zhang[a] and Snezhana Oliferenko[a,b,*]
[a]Temasek Life Sciences Laboratory and [b]Department of Biological Sciences, National University of Singapore, Singapore 117604

ABSTRACT **The fission yeast *Schizosaccharomyces pombe* undergoes "closed" mitosis in which the nuclear envelope (NE) stays intact throughout chromosome segregation. Here we show that Tts1, the fission yeast TMEM33 protein that was previously implicated in organizing the peripheral endoplasmic reticulum (ER), also functions in remodeling the NE during mitosis. Tts1 promotes insertion of spindle pole bodies (SPBs) in the NE at the onset of mitosis and modulates distribution of the nuclear pore complexes (NPCs) during mitotic NE expansion. Structural features that drive partitioning of Tts1 to the high-curvature ER domains are crucial for both aspects of its function. An amphipathic helix located at the C-terminus of Tts1 is important for ER shaping and modulating the mitotic NPC distribution. Of interest, the evolutionarily conserved residues at the luminal interface of the third transmembrane region function specifically in promoting SPB-NE insertion. Our data illuminate cellular requirements for remodeling the NE during "closed" nuclear division and provide insight into the structure and functions of the eukaryotic TMEM33 family.**

Monitoring Editor
Daniel J. Lew
Duke University

Received: Dec 12, 2013
Revised: Jul 7, 2014
Accepted: Jul 22, 2014

INTRODUCTION

Cell growth and division in eukaryotes are supported by complex changes in endomembrane morphology. Membrane remodeling requires generation and stabilization of characteristic curvature and membrane fusion and fission machineries (McMahon and Gallop, 2005; Chernomordik and Kozlov, 2008).

Membranes can be passively deformed due to associated cytoskeletal dynamics (Sheetz, 2001; Grigoriev *et al.*, 2008), as well as by pulling forces exerted by motor proteins (Roux *et al.*, 2005; Wagner *et al.*, 2011). Of importance, curvature can be generated by specialized proteins to compartmentalize membranes and enable membrane trafficking (McMahon and Gallop, 2005). One of the widely used strategies to create curvature is assembly of the arc-like protein scaffolds laterally at the membrane. Typically, coat proteins clathrin, COPI, and COPII that do not exhibit direct binding to lipid bilayers promote vesicle formation by interacting with membrane-associated proteins and polymerizing into cage-like lattices surrounding vesicle membranes (Fotin *et al.*, 2004; Fath *et al.*, 2007; Stagg *et al.*, 2008; Lee and Goldberg, 2010). Many proteins involved in vesicle trafficking contain the concave-shaped Bin–Amphiphysin–Rvs (BAR) domains, which serve as membrane curvature sensing and –stabilizing modules. BAR protein dimers bind to membranes through electrostatic interactions and induce membrane invaginations and protrusions (Rao and Haucke, 2011). General principles in generating and stabilizing membrane curvature, which involve the cytoskeleton, the scaffolding mechanism, and protein–lipid interactions, can be also applied to the shape maintenance of large membrane organelles such as the endoplasmic reticulum (ER), the Golgi apparatus, and the mitochondria (Shibata *et al.*, 2009).

The largest endomembrane organelle, the ER, is an elaborate network of sheets and tubules connected through three-way junctions (Voeltz *et al.*, 2002). The reticulon and DP1/Yop1 proteins function in shaping ER tubules, stabilizing curved edges of ER sheets, and sustaining the reticulated ER network (Voeltz *et al.*, 2006; Hu *et al.*, 2008, 2009; Shibata *et al.*, 2010). Their ER tubulating functions are conserved throughout the eukaryotic domain, from plants to

This article was published online ahead of print in MBoC in Press (http://www.molbiolcell.org/cgi/doi/10.1091/mbc.E13-12-0729) on August 7, 2014.

*Present address: Randall Division of Cell and Molecular Biophysics, King's College London, London SE1 1UL, United Kingdom.

Address correspondence to: Dan Zhang (zhangdan@tll.org.sg), Snezhana Oliferenko (snezhana.oliferenko@kcl.ac.uk).

Abbreviations used: ADEL, ER retention signal sequence; ER, endoplasmic reticulum; INM, inner nuclear membrane; NE, nuclear envelope; NLS, nuclear localization signal; NPC, nuclear pore complex; ONM, outer nuclear membrane; SPB, spindle pole body; TM, transmembrane domain; γ-TuC, γ-tubulin complex.

yeast to animal cells (Voeltz *et al.*, 2006; Sparkes *et al.*, 2010). Proteins from these two families do not exhibit primary sequence similarity but share a similar wedge-shaped membrane topology and self-oligomerization properties favoring membrane tubulation and stabilization of high curvature (Voeltz *et al.*, 2006; Hu *et al.*, 2008; Shibata *et al.*, 2008).

The ER is continuous with the nuclear envelope (NE), which consists of two lipid bilayers termed the outer nuclear membrane (ONM) and the inner nuclear membrane (INM). These two membranes are fused at the sites of nuclear pores, which are decorated by the multisubunit nuclear pore complexes (NPCs; Hetzer, 2010). Similar to the tubular ER, membranes at the nuclear pores exhibit high curvature (Antonin and Mattaj, 2005). Furthermore, in many lower eukaryotes such as the fission yeast *Schizosaccharomyces pombe*, nuclear membranes are highly curved at the so-called NE fenestra that accommodate mitotic microtubule-organizing centers, the spindle pole bodies (SPBs; Ding *et al.*, 1997). Insertion of SPBs within the plane of the NE enables "closed" nuclear division, when the intranuclear mitotic spindle segregates chromosomes within an intact NE (Zhang and Oliferenko, 2013). Of interest, the ER-shaping proteins Rtn1 and Yop1 have been proposed to participate in nuclear pore formation and SPB function in budding yeast (Dawson *et al.*, 2009; Casey *et al.*, 2012).

We showed previously that an evolutionarily conserved TMEM33-family protein, Tts1, functions to sustain the highly curved ER domains in *S. pombe* together with Rtn1 and Yop1. Of note, it can localize to high-curvature ER membranes and execute the ER-shaping function independently of its physical association with Rtn1 and Yop1 (Zhang *et al.*, 2010). However, the molecular mechanisms underpinning its function in ER morphogenesis and other biological activities of Tts1 are not well understood.

In this study, we show that in addition to maintaining the cortical ER network, Tts1 also plays a role in NE remodeling during mitosis. At mitotic onset, Tts1 promotes insertion of the SPBs within the plane of the NE. Furthermore, it sustains the characteristic NE morphology and regular NPC distribution during mitotic nuclear membrane expansion. The latter role of Tts1 in structuring the expanding NE is related to its ER-shaping properties. However, an evolutionarily conserved motif located within the third transmembrane segment has a specific function in promoting formation of the NE fenestra. We identify structural features of Tts1 that are crucial for distinct aspects of mitotic NE remodeling.

RESULTS

Evolutionarily conserved motifs in Tts1 are required for its localization to the tubular ER

Sequence analyses suggest that Tts1 has four transmembrane (TM) regions in the N-terminal half of the protein, followed by a string of three α-helices exposed to the cytosol (Figure 1A; predictions of topology are consistent between www.cbs.dtu.dk/services/TMHMM/ and www.enzim.hu/hmmtop/index.php; Tusnady and Simon, 2001; C-terminal helix predictions are based on Petersen *et al.*, 2009; www.cbs.dtu.dk/services/NetSurfP/). Sequence alignment among proteins from the eukaryotic TMEM33 family revealed two highly conserved motifs (Figure 1A; Bailey *et al.*, 2009; http://meme.nbcr.net/meme/). One motif was found at the luminal interface of the third TM stretch, with a conserved Pro-119 and three aromatic side-chain residues (Tyr-123, His-127, and Tyr-131) predicted to lie on the same side of the helix (Figure 1A; highlighted in yellow). The other conserved, nine–amino acid motif, delimited by two tyrosines (Tyr-203 and Tyr-211), resides in the first of the three cytosolic α-helices (Figure 1A). The positively charged residues (Arg-208/210) within this motif are conserved in fungi (Figure 1A). Although not conserved outside the fission yeast clade, the third C-terminal helix from Val-240 to Ala-257 (VIKNAWHTFKTYVSKFGA) is predicted to exhibit amphipathic properties (Figure 1A; Gautier *et al.*, 2008; http://heliquest.ipmc.cnrs.fr/).

To identify intrinsic signals necessary for localizing Tts1 to the tubular ER, we generated a series of Tts1 mutants based on the predicted protein structure (Figure 1B and Supplemental Figure S1A). Mutant proteins were tagged with green fluorescent protein (GFP) at the C-terminus and expressed under the native *tts1* promoter in *tts1Δ* genetic background. We then analyzed the specificity in their localization to the tubular ER domains marked by Rtn1-mCherry (see *Materials and Methods* for experimental details).

We found that the N-terminal segment of Tts1 containing all transmembrane helices was targeted to the ER but was not enriched in Rtn1-positive membranes, indicating that the C-terminal region was required to confer specific localization of Tts1 to the tubular ER domains (Figure 1B and Supplemental Figure S1A). When we individually deleted each of the predicted C-terminal α-helices in the context of an otherwise wild-type protein, we discovered that only the deletion of the first conserved α-helix resulted in spreading of Tts1 throughout the entire ER (Figure 1B and Supplemental Figure S1A). In line with this, mutating the two conserved arginines lying within this helix to isoleucines was sufficient to abolish Tts1 partitioning to Rtn1-enriched ER domains (Figure 1B and Supplemental Figure S1A).

Of interest, whereas the C-terminal fragment alone did not contain any potential transmembrane regions, it was associated with the ER membranes and accumulated at the lipid droplets, as indicated by its colocalization with the triglyceride lipase Ptl2-mCherry (Figure 1B and Supplemental Figure S1, A and B). This membrane enrichment was abolished when we removed the amphipathic helix at the extreme C-terminus (Supplemental Figure S1B). However, in the context of an otherwise wild-type Tts1, the elimination of this amphipathic helix by either deletion or mutations disturbing its amphipathic properties did not obviously affect Tts1 localization to the tubular ER domains (Figure 1B).

To evaluate whether specific features within the N-terminal transmembrane region of Tts1 were required for its partitioning to curved membranes, we removed an amino acid stretch containing the third and fourth TM helices, which would presumably allow C-terminus to be appropriately exposed to the cytosol. Of interest, the resulting mutant (Tts1-2TM-Cter) localized to the ER but was not enriched in Rtn1-mCherry–marked membranes (Figure 1B and Supplemental Figure S1A), suggesting that this membrane-spanning section was crucial for proper subcellular distribution of the protein. As discussed earlier, the third transmembrane region contains a motif with four evolutionarily conserved residues spaced at equal distances of three amino acids away from each other. This sequence diverged in one of the two *Saccharomyces cerevisiae* TMEM33 paralogues, Per33 (Chadrin *et al.*, 2010), where proline at the position 119 is replaced by serine (Figure 1A). Of interest, the chimeric Tts1-per33 protein where the conserved region was swapped with the corresponding motif derived from Per33 delocalized from the Rtn1-positive domains and spread throughout the entire ER. In contrast, similar replacement with a corresponding Pom33 sequence did not substantially alter Tts1 enrichment at the curved ER membranes (Figure 1B). Yet subcellular distribution of Tts1 was not substantially altered by mutation of the four conserved residues individually or simultaneously (Figure 1B).

Taken together, our data indicated that the last two TM regions and the following cytosolically exposed α-helix were required to

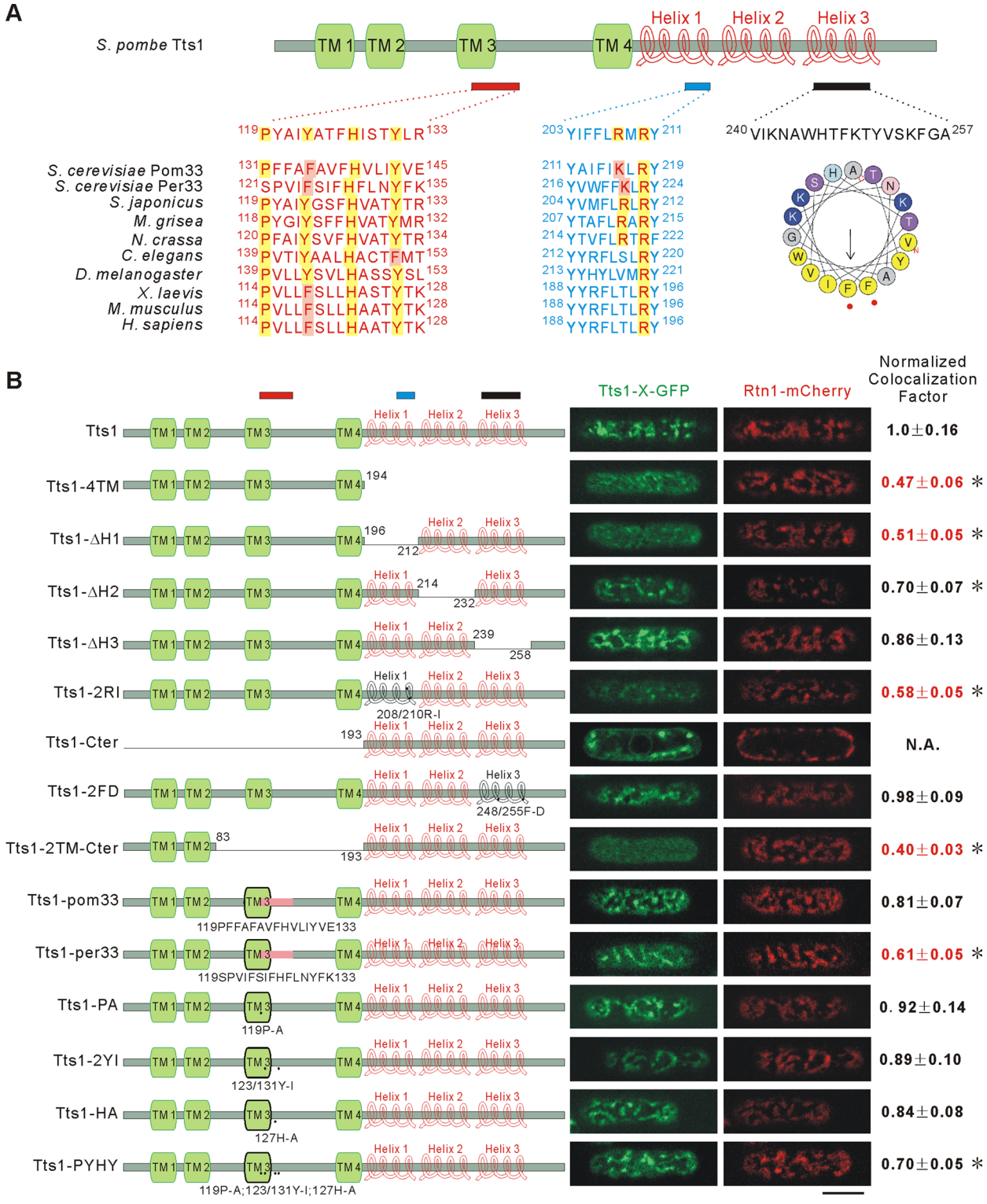

FIGURE 1: Evolutionarily conserved motifs in Tts1 are required for its partitioning to the tubular ER. (A) Predicted structural features and conserved motifs in the TMEM33 protein Tts1 in *S. pombe*. Note that the motif shown in red is conserved throughout the TMEM33 family, whereas the motif in blue contains two charged arginines that are highly conserved among its fungal orthologues. Highlighted are conserved residues that were mutated in this study. The helical wheel showing that helix 3 in Tts1 C-terminus potentially has amphipathic properties was generated using HeliQuest (http://heliquest.ipmc.cnrs.fr/). Mutated residues at the hydrophobic side are indicated by red points. (B) Localization of GFP-fused Tts1 mutants in *tts1*Δ cells expressing Rtn1-mCherry. The cartoons show the logic of construction of Tts1 mutants. Scanning confocal micrographs of cells expressing indicated proteins were taken from either top or middle (for Tts1-Cter) planes of *z*-stacks. Scale bars, 5 μm. Normalized colocalization factors shown in red indicate the significant decrease of specificity in the tubular ER localization of the corresponding Tts1 mutants (mean ± SD; $10 < n < 35$). *$p \ll 10^{-4}$ in comparison to the wild type; two-tailed Student's *t* test.

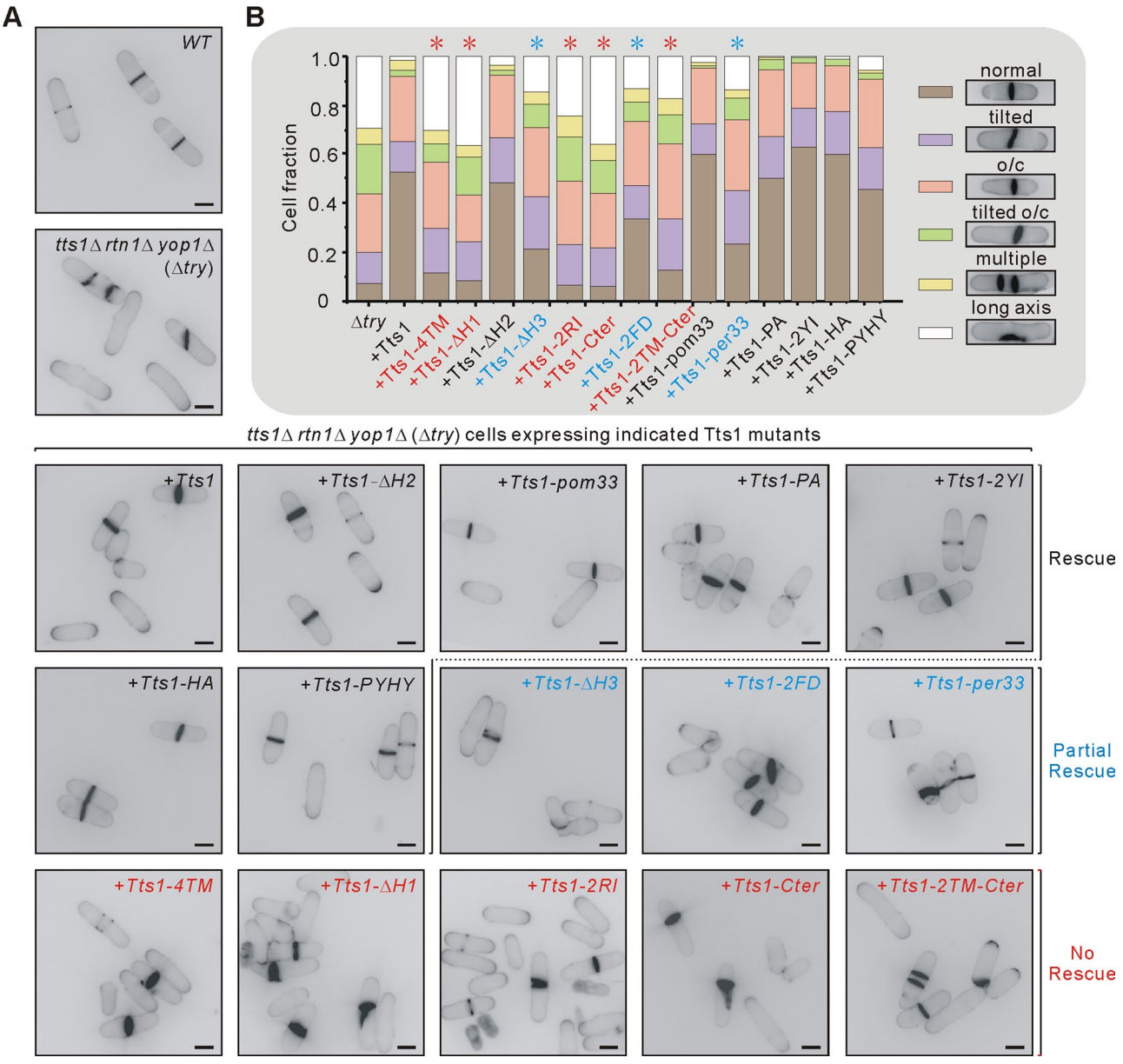

FIGURE 2: Genetic complementation analysis reveals domains important for Tts1 ER-shaping function. (A) Epifluorescence images of Calcofluor-stained cells with indicated genotypes. (B) Quantification of the division septa positioning phenotypes in cells of indicated genetic backgrounds ($500 < n < 1500$). o/c, off-center. Tts1 mutants that did not rescue the division site mispositioning in Δ*try* cells are indicated by red asterisks. Mutants that were partially compromised in correcting division site positioning defects in Δ*try* cells are denoted by blue asterisks.

specify Tts1 localization to the highly curved ER membranes. Incidentally, this segment contains the regions of the highest similarity among eukaryotic TMEM33 proteins.

Localization of Tts1 to the tubular ER and the C-terminal amphipathic helix are required for its functional interaction with the ER-shaping proteins Rtn1 and Yop1

We showed previously that Tts1 functions to sustain the tubular ER structure in *S. pombe* together with Rtn1 and Yop1 (Zhang *et al.*, 2010). Cells lacking all three ER-shaping proteins exhibit severe division-site positioning abnormalities due to conversion of the ER into large, cortically associated sheets, preventing actomyosin ring assembly at the cellular equator (Zhang *et al.*, 2010, 2012). Of note, lack of Tts1, Rtn1, or Yop1 individually also leads to mild division-site mispositioning, but the defects are grossly exacerbated in cells combining either of the two or all three mutations (Zhang *et al.*, 2010). In line with this, when Tts1 was reintroduced into *tts1Δ rtn1Δ yop1Δ* (Δ*try*) background, the severe division-site positioning defects were largely corrected (Figure 2). This system afforded us a genetic tool to examine the available Tts1 mutants with respect to their presumptive ER-shaping function.

To this end, we expressed GFP-fused Tts1 mutants and the wild-type Tts1-GFP in Δ*try* cells and analyzed the accuracy of division-site positioning by staining the cell wall with Calcofluor. In contrast to the wild-type protein, all mutants that were not enriched specifically in the tubular ER failed to rescue the division-site positioning

defects in Δ*try* cells (Figure 2). In line with this, all mutants that corrected division-site mispositioning in Δ*try* cells were enriched in the tubular ER (Figures 1B and 2). Curiously, the mutant proteins that lacked the C-terminal amphipathic helix failed to fully rescue division-site mispositioning in Δ*try* cells in spite of their wild type-like localization to the ER tubules (Figures 1B and 2). This suggested that this amphipathic helix could play a supportive role in shaping the ER membranes in fission yeast.

In conclusion, our genetic complementation analysis suggests that structural features driving association of Tts1 with the highly curved membranes and the C-terminally located amphipathic helix are essential for Tts1 function in organizing the cortical ER network together with Rtn1 and Yop1.

Tts1 is required for structuring the mitotic nuclear envelope

To evaluate whether Tts1 could associate with the highly curved membrane regions at the NE, we used mutant cells lacking the nucleoporin Nup132, the orthologue of the budding yeast Nup133, where the NPCs are abnormally clustered within the NE (Belgareh and Doye, 1997). In *nup132*Δ cells, Tts1-GFP associated with the abnormal NPC clusters marked by Cut11-mCherry, the fission yeast member of Ndc1 nucleoporin family (Supplemental Figure S2A; the cisternal ER protein oligosaccharyltransferase Ost1-GFP served as a control). Cut11 is also enriched at the mitotic SPBs when they are embedded into the NE (West *et al.*, 1998). However, we did not observe specific enrichment of Tts1 at the SPBs at any stage of the cell cycle (Zhang *et al.*, 2010; Supplemental Figure S2B). We concluded that Tts1 associated with the nuclear pores, in addition to its localization to the tubular ER membranes. Similar association between TMEM33-family proteins and the NPCs was observed in a related species, the fission yeast *Schizosaccharomyces japonicus* (Yam *et al.*, 2011, 2013), and in budding yeast (Chadrin *et al.*, 2010).

The NPCs marked by Cut11-GFP remained evenly distributed around the NE throughout mitosis in wild-type *S. pombe*, as the mother nucleus divided into two daughters through a dumbbell-shaped intermediate (Figure 3A, top; the nuclear membrane was labeled by Uch2-mCherry, and Pcp1-mCherry traced the SPBs). Of interest, in 46% of mitotic *tts1*Δ cells, Cut11-GFP clustered in large aggregates at the NE (34 of 74 cells; Figure 3A, bottom) at the stage when the nuclear membrane expanded dramatically to allow formation of the two daughter nuclei (Lim *et al.*, 2007; Yam *et al.*, 2011). These clusters of Cut11-marked NPCs protruded outward during nuclear division (Figure 3A, bottom). The nuclear membrane marker Uch2-mCherry was also present in the protrusions, arguing that these structures represented deformations of the entire NE (Figure 3A, bottom membrane protrusions indicated by arrows). In line with this, we observed similar deformations of the dividing NE using the nuclear basket protein Nup211-GFP, the fission yeast homologue of Mlp1/Tpr known to associate with the inner nuclear side of the NPCs (Strambio-de-Castillia *et al.*, 1999; Bae *et al.*, 2009; 10 of 14 cells; Figure 3B). These NPC-enriched NE extensions did not incorporate into the daughter nuclei (Figure 3, A and B). Yet Cut11 levels at mitotic SPBs or total cellular levels of Cut11 remained unaltered in cells lacking Tts1 (Supplemental Figure S2, C and D). We did not observe abnormal NPC clustering or overt NE shape abnormalities in interphase *tts1*Δ cells (unpublished data).

Of note, NPC clusters in *tts1*Δ cells appeared at the time of mitotic NE expansion when the newly incorporated membranes are presumably remodeled into the functional NE. The ER is the most likely reservoir for this nuclear membrane increase (Anderson and Hetzer, 2007, 2008). Intriguingly, the NPC clusters in mitotic *tts1*Δ cells were found at the junctions between the NE and the peripheral ER, as indicated by visualization of Cut11-GFP and the ER luminal marker mCherry-ADEL (Figure 3C). Similar NE deformations and the NPC aggregates were seen in mitotic cells lacking the major ER tubulating protein Rtn1 (29 of 50 cells; Supplemental Figure S2E and unpublished data), although we did not observe NE morphology abnormalities in cells lacking Yop1 (Supplemental Figure S2E).

We then wondered whether the role of Tts1 in remodeling the mitotic NE was associated with its function in sustaining tubular ER morphology. To this end, we inspected mitotic NPC dynamics in eight point mutants in which *tts1* was mutated at the original locus, among which five retained the ER-shaping function (Tts1-pom33, Tts1-PA, Tts1-2YI, Tts1-HA, and Tts1-PYHY) and three had this function compromised (Tts1-2RI, Tts1-2FD, and Tts1-per33). Mutants that were functional with respect to ER shaping exhibited normal NPC distribution throughout the mitotic NE expansion (Supplemental Figure S2F). On the contrary, a considerable proportion of *tts1-2RI*, *tts1-2FD*, and *tts1-per33* cells that were compromised in maintaining the tubular ER domains displayed mild but reproducible NPC clustering defects during NE division (seven of 15 cells for *tts1-2RI*, seven of 12 cells for *tts1-2FD*, and six of 11 cells for *tts1-per33*; Supplemental Figure S2F).

Collectively our data suggest that Tts1 functions in maintaining proper architecture of the dividing NE. This role of Tts1 appears to be related to its function in structuring the cortical ER network.

Tts1 assists Cut11 in mitotic spindle assembly

The SPBs in *S. pombe* exhibit a cycle of NE insertion and extrusion during mitosis (Ding *et al.*, 1997), suggesting tight spatiotemporal coordination between SPB anchorage and nuclear membrane remodeling. Fusion between the ONM and INM generating the NE fenestra is necessary for the NE insertion of mitotic SPBs (Jaspersen and Ghosh, 2012).

Cut11 is an essential nucleoporin that is enriched at the mitotic SPBs when they are embedded within the NE (West *et al.*, 1998). At the restrictive temperature of 36°C, cells carrying the temperature sensitive (ts) alleles of *cut11* do not properly insert the mitotic SPBs in the NE and fail to form bipolar spindles and complete mitosis (West *et al.*, 1998; Figure 4A). Curiously, we initially identified Tts1 as a high-copy suppressor of a tight temperature-sensitive allele of *cut11*, *cut11-6*, which carries a missense mutation causing Thr-to-Ile substitution at position 498 (Figure 4B and Supplemental Figure S3A). Of interest, among the other five previously isolated *cut11* ts mutants, that is, *cut11-1* to *cut11-5* (West *et al.*, 1998; Supplemental Figure S3A), increase in Tts1 levels could also suppress *cut11-2/3/4/5* but not *cut11-1* at 36°C (Supplemental Figure S3B). At the same time, *tts1*Δ displayed negative genetic interactions with all six *cut11* ts alleles, including *cut11-1*, albeit in a milder manner as compared with the rest (Figure 4C and Supplemental Figure S3C).

To evaluate the mitotic spindle structure in live *cut11-6* and *cut11-6 tts1*Δ cells, we visualized microtubules, the SPBs, and the nucleoplasm by the GFP-tagged α-tubulin Atb2, Pcp1-mCherry, and an artificial nuclear marker protein, GST-NLS-mCherry, respectively. Quantification of the spindle-related phenotypes was performed in fixed cells stained with anti–α-tubulin antibody. At the permissive temperature of 24°C, only 27.3% of mitotic *cut11-6 tts1*Δ cells exhibited bipolar spindles, as compared with 56.7% of cells carrying *cut11-6* alone (Figure 4, D and E; $n = 300$ for all backgrounds). Furthermore, we observed a noticeable increase in the incidence of mitotic cells exhibiting either defective monopolar spindles or no microtubules at all when *cut11-6* and *tts1*Δ mutations

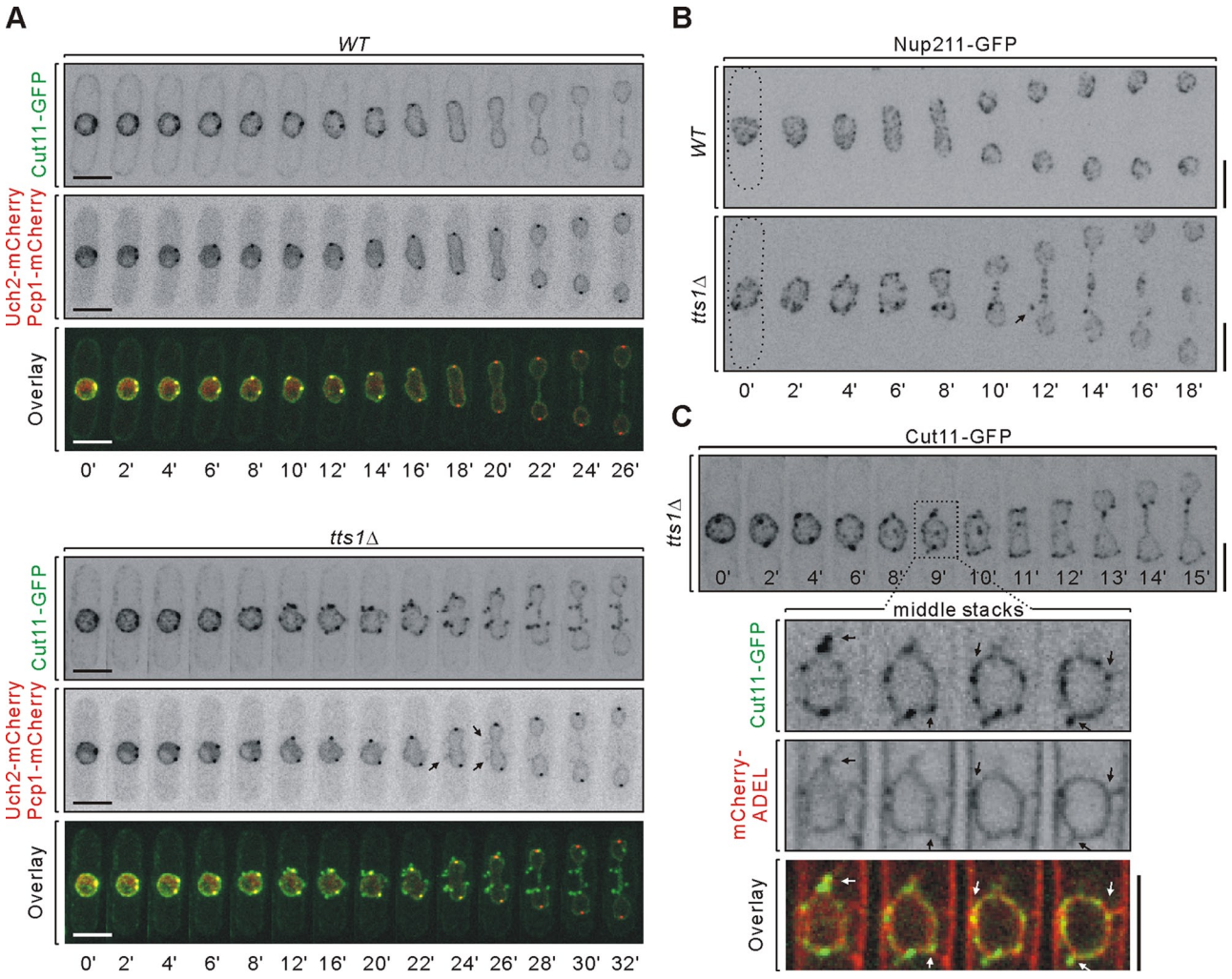

FIGURE 3: Tts1 is required for maintaining normal morphology of the dividing nuclear envelope. (A, B) Time-lapse maximum *z*-projection images of wild-type (*WT*) and *tts1*Δ cells coexpressing indicated marker proteins. The abnormal NE protrusions are marked by arrows. (C) Time-lapse maximum *z*-projection images of *tts1*Δ cells coexpressing the artificial luminal ER marker protein mCherry-ADEL and Cut11-GFP. Bottom, middle stacks from the framed region with 2× magnification. The clusters of Cut11-marked NPCs at the ER-NE junctions are indicated by arrows. The elapsed time is shown in minutes. Scale bars, 5 μm.

were combined (Figure 4, D and E). Of note, at the restrictive temperature of 36°C, a significant proportion of mitotic *cut11-6 tts1*Δ cells (36%) failed to nucleate spindle microtubules (Figure 4E). Most *tts1*Δ cells formed normal bipolar spindles (Figure 4, D and E), but a minor fraction of mitotic *tts1*Δ cells exhibited no spindles or very short, abnormal-looking spindles (Figure 4E and Supplemental Figure S3D), suggesting that Tts1 could have a marginal role in mitotic spindle assembly.

Taken together, our genetic data suggest that Tts1 could play a role in assisting Cut11 in bipolar spindle formation during mitosis.

Mitotic SPBs are compromised in recruiting the γ-tubulin complex in *cut11-6 tts1*Δ cells

To examine mitotic spindle formation carefully, we performed time-lapse analyses of cells expressing fluorescent protein markers for the spindle (GFP-Atb2), the SPBs (Pcp1-mCherry), and the nucleoplasm (GST-NLS-mCherry) at 24°C. Wild type cells initiated bipolar spindle assembly within 3 min (2.5 ± 0.8 min, n = 11) after depolymerization of the interphase microtubule arrays (Figure 5A). *tts1*Δ cells assembled short spindles 2.8 ± 2.0 min (n = 18) after the depolymerization of cytoplasmic microtubules. However, in line with our immunofluorescence data, some *tts1*Δ cells went through a short but noticeable stage with microtubules forming small, aster-like structures (seven of 18 cells, indicated by an arrow in Figure 5A). All *tts1*Δ cells subsequently assembled bipolar spindles and completed mitosis.

Spindle microtubule nucleation was slightly delayed in single *cut11-6* mutant cells at the permissive temperature of 24°C (we observed monopolar spindles appearing 4.8 ± 2.0 min after disassembly of cytoplasmic microtubule arrays, n = 6; Figure 5A). However, deletion of *tts1* in *cut11-6* genetic background led to a significant delay in mitotic microtubule nucleation and spindle assembly (spindle microtubules appeared 15.0 ± 8.6 min after depolymerization of interphase microtubule arrays, n = 8; Figure 5A). Of interest, although we did not observe spindle microtubules, two SPBs in *cut11-6 tts1*Δ cells eventually separated to some extent. Subsequently, microtubule nucleation was initiated asymmetrically from one of the two SPBs (Figure 5A, bottom). Because the old (mother)

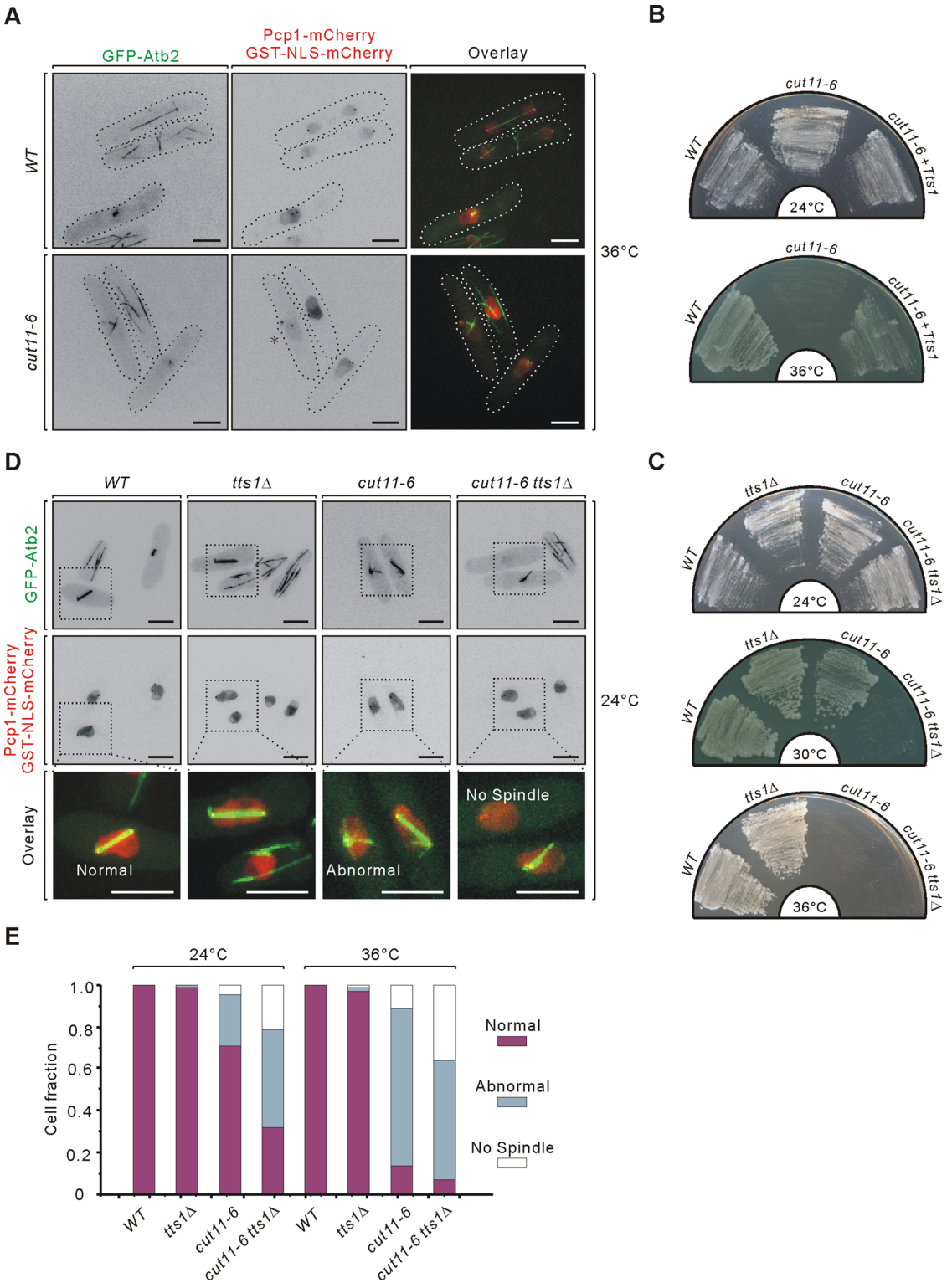

FIGURE 4: Tts1 functions with Cut11 in bipolar spindle formation. (A) Morphology of microtubule arrays including the mitotic spindles (marked by GFP-Atb2) and the SPBs (marked by Pcp1-mCherry) in *WT* and *cut11-6* cells at the restrictive temperature of 36°C. Nuclear integrity is monitored by localization of the artificial nucleoplasmic marker GST-NLS-mCherry. Cells were shifted from 24 to 36°C at 2 h before imaging. Note that nuclear integrity is lost in *cut11-6* cells during mitosis (denoted by an asterisk). Shown are the maximum projections of *z*-stacks obtained from spinning disk confocal microscopy. (B) Extra copy of *tts1* enables *cut11-6* cells to grow at 36°C. (C) *cut11-6 tts1*Δ cells fail to form colonies at the intermediate temperature of 30°C when a single *cut11-6* mutant grows normally. (D) Maximum *z*-projection images of spinning disk confocal stacks of cells with indicated genetic backgrounds coexpressing GFP-Atb2, Pcp1-mCherry and GST-NLS-mCherry at 24°C. (E) Quantification of spindle-related phenotypes was performed in fixed cells of the indicated genetic backgrounds at 24 and 36°C ($n = 300$). Cells were shifted from 24 to 36°C at 3 h before fixation. Three categories of spindle morphologies are defined in magnified views of cells in D. Scale bars, 5 μm.

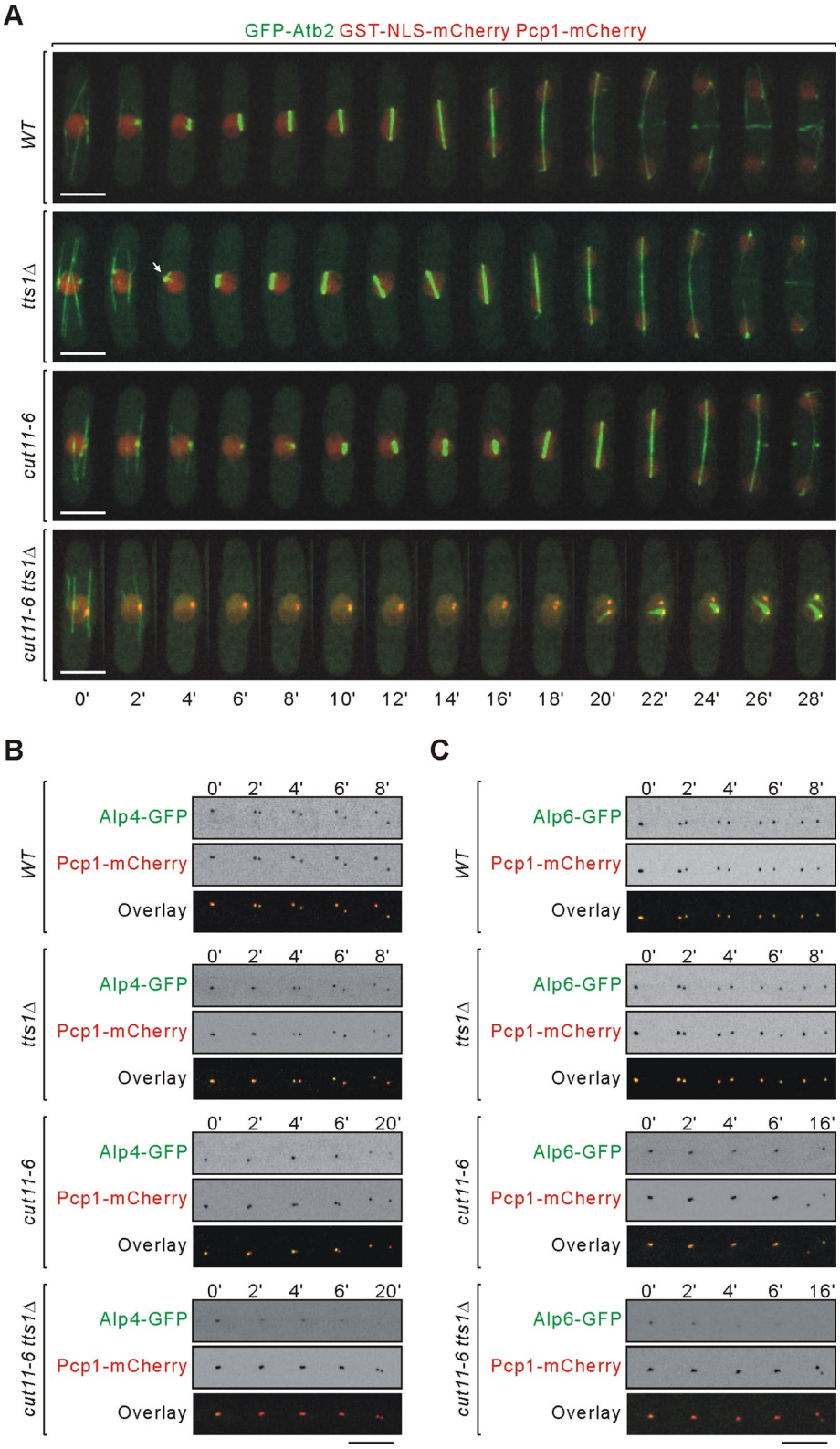

FIGURE 5: The mitotic SPBs are compromised in recruiting the γ-tubulin complex in *cut11-6 tts1*Δ cells. (A) Time-lapse maximum *z*-projection images of spinning disk confocal stacks of cells with indicated genetic backgrounds coexpressing GFP-Atb2, Pcp1-mCherry, and the nucleoplasm marker protein GST-NLS-mCherry. An aster-like short spindle in early mitotic *tts1*Δ cells is denoted by an arrow. (B, C) Time-lapse maximum *z*-projection images of spinning disk confocal stacks of cells with indicated genetic backgrounds coexpressing Pcp1-mCherry and Alp4-GFP (B) or Alp6-GFP (C). Cells were grown and imaged at 24°C, the permissive temperature for *cut11-6* mutant. The elapsed time is shown in minutes. Scale bars, 5 μm.

and new (daughter) SPBs differ in their potential to nucleate microtubules in several spindle-defective mutants (Tallada *et al.*, 2009; Fong *et al.*, 2010; Tamm *et al.*, 2011), we wondered whether SPB age could account for asymmetric microtubule nucleation in *cut11-6 tts1*Δ cells. We used the slow-folding red fluorescent protein (RFP)–tagged Pcp1 to differentiate between old and new SPBs (Grallert *et al.*, 2004). Sid2-GFP and GFP-Atb2 were used to trace both SPBs and visualize spindle microtubules. However, we found that in *cut11-6 tts1*Δ cells, the monopolar spindles could be nucleated from either mother (41 of 74 cells) or daughter SPB (33 of 74 cells; Supplemental Figure S4A).

In *S. pombe*, SPB recruitment of the mitotic regulator Cut12 (Bridge *et al.*, 1998) and the polo kinase Plo1 (Ohkura *et al.*, 1995; Bahler *et al.*, 1998) is required for SPB-NE insertion and SPB activation (Tallada *et al.*, 2009; Fong *et al.*, 2010). Therefore, we examined whether a pronounced delay in spindle microtubule nucleation in *cut11-6 tts1*Δ cells was caused by failure to recruit Plo1 or Cut12 on the SPBs. However, we found that both Plo1 and Cut12 were normally loaded to the mitotic SPBs in *cut11-6 tts1*Δ cells (Supplemental Figure S4B).

The γ-tubulin complex (γ-TuC) is the core of the cellular microtubule nucleation machinery and is required for spindle assembly (Horio *et al.*, 1991; Zheng *et al.*, 1995; Moritz and Agard, 2001). The essential components of the γ-TuC in fission yeast include γ-tubulin and two accessory proteins, Alp4 (the GCP2/Spc97 orthologue) and Alp6 (the GCP3/Spc98 orthologue; Vardy and Toda, 2000). All of these components have been shown to localize to the SPBs at all cell cycle stages (Horio *et al.*, 1991; Ding *et al.*, 1997; Vardy and Toda, 2000).

As expected, both Alp4-GFP and Alp6-GFP localized to the mitotic SPBs marked by Pcp1-mCherry in wild-type cells (Figure 5, B and C). We did not observe any abnormalities in their localization in the absence of Tts1 (Figure 5, B and C). However, we found that both Alp4-GFP and Alp6-GFP were frequently absent from one of the mitotic SPBs in *cut11-6* cells already at the permissive temperature of 24°C (Figure 5, B and C; 18 of 28 cells and 24 of 50 cells, respectively). Deletion of *tts1* in *cut11-6* genetic background considerably aggravated this phenotype. During interphase in the double-mutant cells, the γ-tubulin complex components localized normally to SPB, but as cells entered mitosis, the fluorescence intensity of Alp4-GFP and Alp6-GFP at SPBs

dramatically decreased. Nearly 94% of early mitotic *cut11-6 tts1*Δ cells lost Alp4-GFP from one or both SPBs (Figure 5B; $n = 48$). Similarly, 77% of early mitotic cells did not localize Alp6-GFP to one or both SPBs (Figure 5C; $n = 48$). The failure to observe the γ-tubulin complex at the mitotic SPBs was not due to fluorophore photobleaching, as we could readily visualize recruitment of both Alp4-GFP and Alp6-GFP to SPBs at the later time points (Supplemental Figure S4C).

Therefore, γ-TuC localization to the mitotic SPBs was severely compromised in *cut11-6 tts1*Δ cells already at the permissive temperature of 24°C, potentially explaining a significant delay in spindle microtubule nucleation.

Tts1 functions in NE fenestration to facilitate mitotic SPB insertion

In closed mitosis, the nuclear membrane is rapidly remodeled to fenestrate the NE and enable integration of the duplicated SPBs in the NE without breaching the nucleocytoplasmic barrier (Gonzalez *et al.*, 2009; Tallada *et al.*, 2009). Cells deficient in Cut11 function lose nuclear integrity and exhibit large gaps in the NE adjacent to SPBs upon unproductive SPB insertion (Tallada *et al.*, 2009; Figure 4A; a cell in which the nuclear integrity is lost is indicated with an asterisk). In line with this, we observed leakage of the artificial nuclear marker GST-NLS-mCherry into the cytoplasm in mitotic *cut11-6* cells at the restrictive temperature of 36°C (Figure 6A; 10 of 10 cells). Of interest, mitotic *cut11-6 tts1*Δ cells frequently maintained NE integrity (Figure 6A; four of eight cells). In these cells, spindle microtubules were not nucleated from the SPBs throughout the course of imaging, consistent with our immunofluorescence data (Figure 4E).

Of interest, the mitotic SPBs in the double mutant cells were frequently found adjacent to nuclear membrane projections marked by the artificial luminal ER marker GFP-ADEL (24 of 26 cells; Figure 6B). To further investigate this phenotype, we performed serial section electron microscopy (EM) analysis on early mitotic *cut11-6 tts1*Δ cells that were harvested after 3-h incubation at the restrictive temperature of 36°C. The EM revealed that the two mitotic SPBs were not integrated within the plane of the NE. Instead, they were typically found within a NE bleb that appeared to expand within a perinuclear space between the outer and inner nuclear membranes, suggesting that NE fenestration was incomplete (Figure 6C; see Supplemental Figure S5 for the full series; $n = 7$ cells).

Taken together, our results suggest that Tts1 promotes mitotic SPB insertion by modulating fenestration of the nuclear membrane.

Evolutionarily conserved TMEM33 motifs are required for Tts1 function in promoting mitotic SPB-NE interaction

We wondered whether the role of Tts1 in mitotic SPB-NE interaction was related to its ER-shaping function. It is possible that the ER-shaping proteins could contribute to NE fenestration and/or SPB integration into the NE by stabilizing the highly curved membranes at the edges of the emerging fenestrae. Thus it is conceivable that Rtn1 and Yop1 could function similarly to Tts1 with respect to mitotic spindle dynamics. However, deletion of either *rtn1* or *yop1* in *cut11-6* genetic background did not lead to exacerbation of spindle-related phenotypes (Supplemental Figure S6), suggesting that Tts1 had a specific role in this process.

To determine domains important for Tts1 function in the context of mitotic SPB-NE interaction and spindle assembly, we performed complementation analyses by introducing the *tts1* mutants described earlier (Figure 1) into the *cut11-6* tts1Δ genetic background. All mutants that failed to partition to the ER tubules did not rescue spindle defects in *cut11-6 tts1*Δ cells (Figure 7A), suggesting that the structural traits specifying localization of Tts1 to the curved ER membranes may be pertinent to its function in SPB-NE insertion. However, the mutant Tts1 proteins where the C-terminal amphipathic helix was disrupted fully rescued the spindle defects in *cut11-6 tts1*Δ cells in spite of their compromised tubular ER-shaping function (Figure 7A). Moreover, point mutations (P119A, Y123/131I, and H127A) in the conserved residues within the third membrane-spanning region of Tts1 that did not lead to obvious ER architecture defects (Figures 1 and 2, Supplemental Figure S2F, and unpublished data) rendered Tts1 nonfunctional with respect to mitotic spindle assembly (Figure 7A). These observations suggested that the role of Tts1 in promoting SPB insertion was distinct from its functions in sustaining the ER morphology.

To conclude, our results suggest that the TMEM33-family protein Tts1 functions in mitotic remodeling of the NE in addition to its role in shaping the peripheral ER. The structural features indispensable for localizing Tts1 to the highly curved ER domains are essential for its membrane-remodeling activities. Of interest, whereas the C-terminal amphipathic helix is required for structuring the cortical ER and an expanding mitotic NE, the highly evolutionarily conserved residues in the third transmembrane region contribute specifically to Tts1 function in modulating formation of the SPB fenestrae and spindle assembly (Figure 7B).

DISCUSSION

Our structure–function analyses revealed structural features of Tts1 that are important for its enrichment at the highly curved ER membranes. The central region of the protein comprising TM3 and TM4 together with an evolutionarily conserved α-helix 1 is required for Tts1 association with the tubular ER. Replacement of the two conserved arginines (Arg-208/210) in the cytosolic helix 1 with noncharged isoleucines delocalizes Tts1 from the high-curvature ER domains and abolishes its function in sustaining the ER morphology (Figures 1 and 2). Structural studies of membrane proteins suggest that the charged residues alone or in combination with polar residues are frequently involved in polar interactions with the lipid head groups (Palsdottir and Hunte, 2004; Contreras *et al.*, 2011). It is possible that the conserved arginines could orient helix 1 at the membrane and promote curvature in combination with the adjoining TM region. Curiously, whereas the stretch of amino acids flanking TM3 is important for Tts1 localization, mutations of four evolutionarily conserved residues at this region did not affect the protein's partitioning to the tubular ER or its function in ER shaping (Figures 1 and 2).

Amphipathic helices are widely used in generating curved cellular membranes (McMahon and Gallop, 2005; Shibata *et al.*, 2009). Insertion of nonpolar residues of an amphipathic helix into the hydrophobic core of the lipid bilayer displaces polar head groups, reorienting acyl chains and hence inducing the curvature. Of interest, the C-terminal amphipathic feature is not necessary for localizing Tts1 to the tubular ER, yet it plays a role in sustaining the tubular domains (Figures 1 and 2). It is possible that initial partitioning of Tts1 to the tubular ER would allow the amphipathic helix to function locally in promoting high membrane curvature. Such cooperation between the transmembrane region and the C-terminal amphipathic helix in maintaining the ER morphology has been proposed for the dynamin-like GTPase atlastin/Sey1 (Hu *et al.*, 2009; Orso *et al.*, 2009; Liu *et al.*, 2012).

The closed mitosis for which the nuclear volume remains constant requires bulk nuclear membrane insertion to accommodate

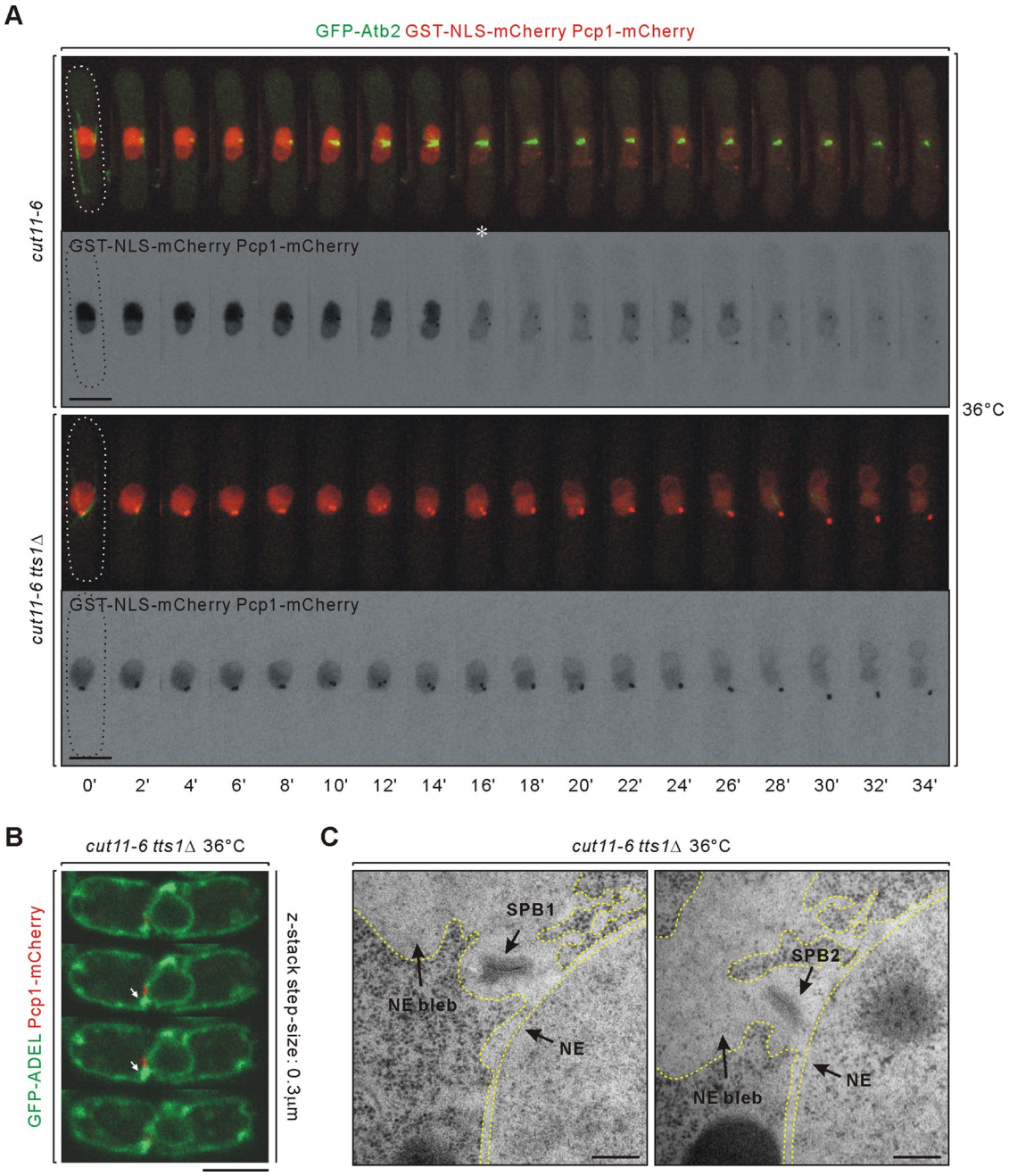

FIGURE 6: Tts1 promotes formation of the SPB fenestrae. (A) Time-lapse maximum *z*-projection images of spinning disk confocal stacks of *cut11-6* or *cut11-6 tts1*Δ cells coexpressing indicated marker proteins at 36°C. The temperature was shifted from 24 to 36°C at 3 h before imaging. Loss of the NE integrity is indicated by leakage of the artificial nucleoplasmic marker GST-NLS-mCherry into cytoplasm in *cut11-6* cells (denoted by an asterisk). The elapsed time is shown in minutes. (B) Scanning confocal micrographs of *cut11-6 tts1*Δ cells coexpressing Pcp1-mCherry and GFP-ADEL. The temperature was shifted from 24 to 36°C at 3 h before imaging. Shown are four serial planes from a *z*-stack with a step size of 0.3 μm. White arrows denote NE projection adjacent to the two mitotic SPBs. Scale bars, 5 μm. (C) Micrographs representing two sections of a *cut11-6 tts1*Δ cell where the mitotic SPBs are positioned within a NE bleb. Membrane boundaries are indicated by yellow dashed lines. NE, nuclear envelope; SPB, spindle pole body. Scale bars, 200 nm.

chromosome segregation and formation of the two daughter nuclei (Lim *et al.*, 2007; Yam *et al.*, 2011). The peripheral ER that is continuous with the ONM most likely serves as a membrane reservoir for nuclear expansion (Anderson and Hetzer, 2007, 2008). Intriguingly, we observed unusual deformations of the NE during mitosis in *tts1* mutant cells that are compromised in ER-shaping function. These deformations are manifested as the NPC-rich extensions of the NE connected to the peripheral ER (Figure 3 and Supplemental Figure S2F). Similar abnormal structures also appear in cells lacking the ER-tubulating protein Rtn1 (Supplemental Figure S2E). These structures could form as a result of invasion of NE proteins into the ER/NE junctions that are probably the sites of membrane incorporation

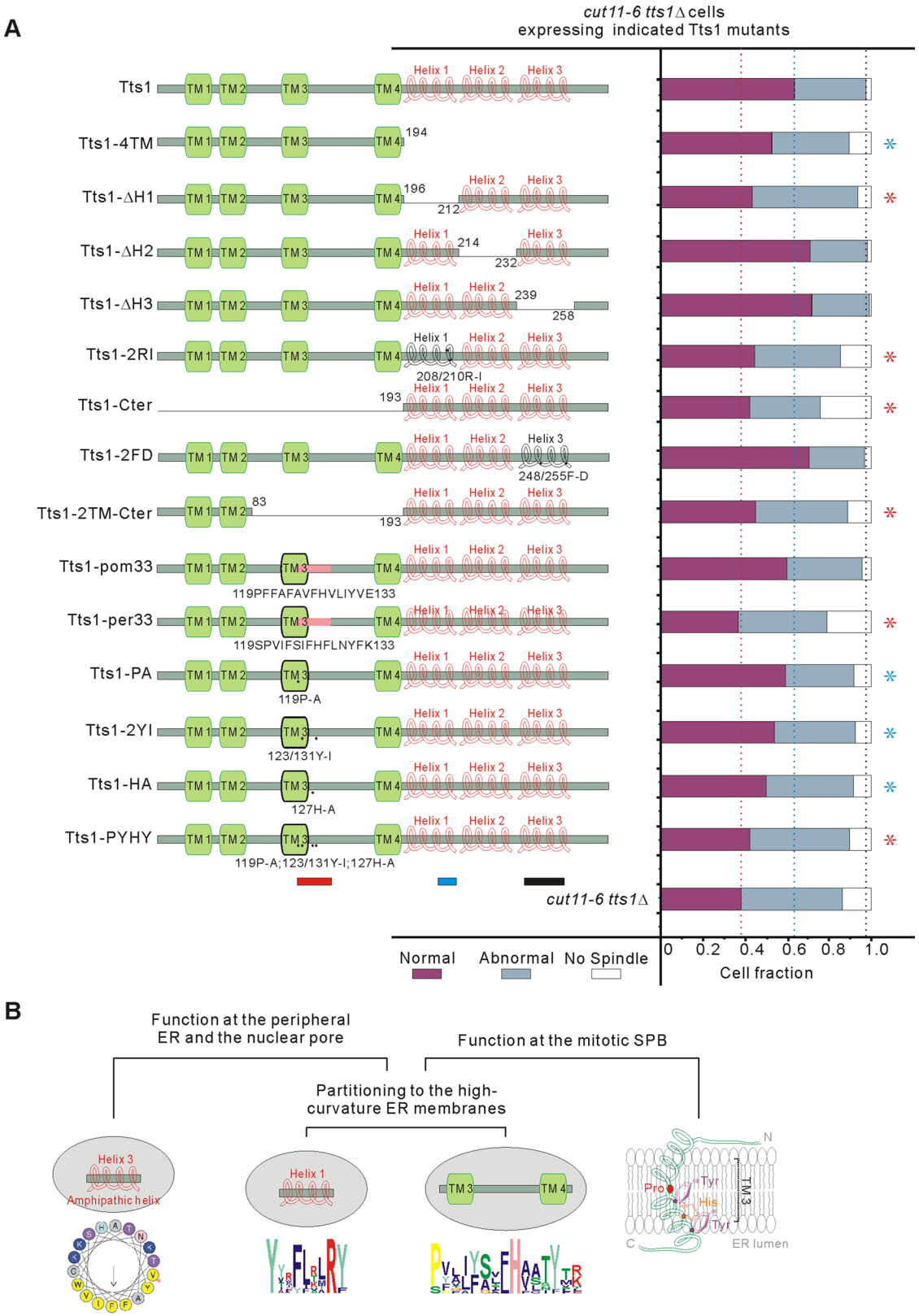

FIGURE 7: Evolutionarily conserved TMEM33 motifs are required for Tts1 function in SPB-NE interaction and spindle assembly. (A) Quantification of spindle morphologies in cells with the indicated genetic backgrounds at 24°C ($n = 500$). Spindle morphologies are categorized as in Figure 4D. The red asterisks highlight Tts1 mutants that were unable to rescue spindle defects in *cut11-6 tts1*Δ cells. Tts1 mutants that were partially compromised in correcting spindle abnormalities in *cut11-6 tts1*Δ cells are indicted by blue asterisks. (B) Diagram showing structural features of Tts1 important for its functions in structuring the cortical ER and the mitotic NE and in the mitotic SPB-NE insertion. A possible topology of the third transmembrane domain (TM3) with four conserved residues is shown as well.

during mitosis. It is possible that compromising the membrane remodeling could affect maintenance of the ER/ONM boundary during the rapid NE expansion phase. The ER-shaping properties of Tts1 and Rtn1 could contribute to regulating the nuclear pore distribution during rapid NE growth. Alternatively, the altered morphology of the peripheral ER observed in *rtn1*Δ and *tts1*Δ mutant cells could indirectly influence remodeling of the expanding NE during mitosis.

NE fenestration and SPB insertion into the fenestrae are well coordinated in *S. pombe*, so that nuclear membrane integrity is maintained at all times (Gonzalez *et al.*, 2009; Tallada *et al.*, 2009). The delay in either step could result in abnormal breaching of the NE in the vicinity of the SPBs and/or late spindle formation (Tallada *et al.*, 2009; Tamm *et al.*, 2011). Failure to nucleate spindle microtubules in the double-mutant *cut11-6 tts1*Δ cells appears to be directly related to a defect in SPB-NE insertion. Indeed, it has been proposed that the pericentrin protein Pcp1, which anchors the γ-tubulin complex at the SPBs during mitosis, does not contain the nuclear localization signal and therefore requires the SPB-NE insertion event to enter the nucleus and organize the nuclear γ-TuC (Flory *et al.*, 2002). Transient delocalization of the γ-TuC from the mitotic SPBs in *cut11-6 tts1*Δ cells already at the permissive temperature (Figure 5, B and C) could be a manifestation of SPB insertion delay. In line with this, our EM data clearly show that the mitotic SPBs fail to insert into the NE when functions of both Cut11 and Tts1 are compromised (Figure 6C and Supplemental Figure S5). Intriguingly, these SPBs appear trapped within a locally expanded perinuclear space, with the outer nuclear membrane forming flares facing the cytoplasm (Figure 6C and Supplemental Figure S5). Such topology could result from failure to fuse the two membrane layers at the site of SPB insertion. Arguing that Tts1 has a specific role in membrane remodeling during SPB insertion, this phenotype has not been observed in either *cut11* single mutants (West *et al.*, 1998; Tallada *et al.*, 2009) or other mutants defective in SPB insertion (Fong *et al.*, 2010; Tamm *et al.*, 2011).

Studies in budding yeast suggested that the ER-tubulating proteins are involved in both NPC biogenesis and SPB function (Dawson *et al.*, 2009; Casey *et al.*, 2012). Surprisingly, whereas Tts1 function in regulating NPC distribution in the mitotic NE is related to its ER-shaping properties (Supplemental Figure S2F), its role in promoting mitotic SPB-NE interaction appears clearly distinct (Figures 2 and 7). In line with this, depletion of the ER-tubulating protein Rtn1 or Yop1 does not exacerbate spindle defects in *cut11-6* cells (Supplemental Figure S6). Therefore, formation of the NE fenestrae for mitotic SPB insertion may not be mechanistically identical to the generation of the ER tubules or the nuclear pores.

Membrane fusion and curvature can be generated by modulating the distribution of fusogenic lipids within the lipid bilayer (Chernomordik and Kozlov, 2003). Of interest, alteration in nuclear membrane composition has been suggested to affect SPB duplication and function in budding yeast (Witkin *et al.*, 2010). Furthermore, the integral membrane protein Brr6, which promotes NE remodeling during SPB insertion and extrusion in *S. pombe*, has been implicated in maintaining cellular lipid homeostasis (Hodge *et al.*, 2010; Tamm *et al.*, 2011). Because Tts1 is not enriched at the mitotic SPBs (Supplemental Figure S2B) and does not physically interact with Cut11 (unpublished data), we propose that it could function in a broader context of regulating membrane composition and dynamics of the NE/ER system. Indeed, we observed an increase in cellular phosphatidylethanolamine-to-phosphatidylcholine ratio in cells lacking Tts1 (unpublished data). Of interest, the evolutionarily conserved residues Pro-119, Tyr-123, His-127, and Tyr-131 at the luminal interface of the TM3 are crucial for the SPB-related function (Figure 7). Aromatic amino acids have been shown to stabilize the lipid–protein interaction (Palsdottir and Hunte, 2004), and it is tempting to speculate that the aromatic side chains of Tyr-123, His-127, and Tyr-131, which presumably align at the same side of the transmembrane α-helix (Figure 7B), could engage in lipid–protein interactions. In principle, these residues could potentially mediate cation–π interactions, hydrogen bond formation, and proton transfer. Of note, placing of proline within the motif could be critical for Tts1 function, since the chimeric protein Tts1-per33 where proline is shifted by one amino acid was fully incompetent in promoting SPB insertion (Figure 7). Further investigation of structural and biochemical properties of this highly conserved motif with respect to lipid interaction and/or possible enzymatic activity will provide insights into the molecular functions of the TMEM33 family.

MATERIALS AND METHODS

S. pombe strains, reagents, and constructs

S. pombe strains used in this study and their genotypes are listed in Supplemental Table S1. Media for vegetative growth and genetic methods were as described in Gould (2004). Genetic crosses and sporulation were performed on yeast extract/peptone/dextrose agar plates. To induce the NPC clustering phenotypes in *nup132*Δ background, cells shown in Supplemental Figure S2A were grown on minimal-medium plates with full supplements. Cell wall stain Calcofluor White was obtained from Sigma-Aldrich (St. Louis, MO). The coding sequences of C-terminally GFP-fused Tts1 mutants listed in Figure 1B and Supplemental Figure S1B were integrated into the *leu1* genomic locus under the *tts1* native promoter. Integration at the *leu1* locus did not affect abundance of the full-length Tts1 since Tts1-GFP expressed from its native chromosomal locus exhibited comparable protein levels (Supplemental Figure S1C). Compared to wild-type Tts1, Tts1 mutants were detected at either higher or comparable protein levels (Supplementary Figure S1C). Of importance, there was no correlation between protein abundance and localization or functions of Tts1 mutants. Thus it appears that functional variance among Tts1 mutants cannot be attributed to differences in cellular protein abundance. The pJK210-based constructs containing specific *tts1* point mutations were used for integration at the *tts1* genomic locus, and the resulting untagged *tts1* mutants shown in Supplemental Figure S2F were confirmed by sequencing analyses. The artificial nucleoplasmic marker GST-NLS-mCherry derived from pREP81-GST-NLS-GFP, which was kindly provided by Masamitsu Sato (University of Tokyo, Tokyo, Japan), was expressed from the nmt81 promoter at the *leu1* locus. Plasmids were constructed using standard molecular biology techniques.

Multicopy suppressor screening

cut11-6 cells were transformed with a fission yeast high-copy plasmid genomic library. Cells were plated on leucine-deficient minimal-medium plates and incubated at 24°C. When tiny colonies started to emerge, plates were shifted to 36°C. Plasmids were isolated from the healthy, growing colonies at 36°C and sequenced to identify the suppressors. To confirm the suppression, engineered plasmids that only contained the potential suppressors were retransformed into *cut11-6* mutant cells.

Immunofluorescence staining

Cells were fixed with 3.7% formaldehyde and spheroplasted using lysing enzymes (Sigma) and Zymolyase (Nacalai Tesque, Kyoto, Japan) in 1.2 M sorbitol in phosphate-buffered saline (PBS).

Permeabilization was performed in 1% Triton X-100 in PBS. PBAL (1 mM sodium azide, 50 μg/ml carbenicillin, 1% bovine serum albumin, and 100 mM lysine hydrochloride in PBS) was used for blocking and for incubation with primary and secondary antibodies. The anti–α-tubulin antibody TAT-1 was a gift from K. Gull (University of Oxford, Oxford, United Kingdom).

Electron microscopy

Electron microscopy was performed using high-pressure frozen and freeze-substituted cells as described by Giddings *et al.* (2001). Briefly, cells were harvested from liquid culture by vacuum filtration, transferred to an aluminum specimen carrier (Techno-Trade, Manchester, NH), and frozen with a stream of nitrogen at a pressure of 1000 bar. Frozen samples were freeze-substituted into acetone containing 2% osmium tetroxide and 0.3% uranyl acetate at –90°C over 2 d, warmed to –20°C, held at this temperature for 3 h, and then warmed to room temperature over 2 h. Fixed samples were rinsed in acetone and gradually infiltrated into Epox-Araldite (Electron Microscopy Sciences, Port Washington, PA). Serial sections (75 nm) were collected onto formvar-coated copper slot grids (EMS) and poststained with 2% uranyl acetate and Reynold's lead citrate. Serial sections were imaged with an FEI-Philips CM100 electron microscope (Mahwah, NJ) operating at 80 kV and data recorded with an AMT camera (Deben, Bury St Edmunds, United Kingdom).

Microscopy

Epifluorescence still images were collected using a mercury lamp as an illumination source with appropriate sets of filters on a Zeiss Axiovert 200M (Plan Apochromat 100×/1.4 numerical aperture [NA] objective lens; Carl Zeiss, Gottingen, Germany) microscope equipped with CoolSnap camera (Photometrics, Tucson, AZ) and Uniblitz shutter driver (Photonics, Rochester, NY) under the control of a MetaMorph software package (Universal Imaging, West Chester, PA).

Scanning confocal microscopy was performed on a LSM510 microscope (Carl Zeiss) equipped with Achroplan 100×/1.25 NA objective lens, a 488-nm argon laser (for GFP excitation), and a 543-nm HeNe laser (for mCherry excitation). Time-lapse fluorescence microscopy images were generated on a Zeiss Axiovert 200M microscope equipped with UltraView RS-3 confocal system: CSU21 confocal optical scanner and 12-bit digital cooled Hamamatsu Orca-ER camera (OPELCO, Sterling, VA). The *z*-stack maximum projection images were obtained by MetaMorph built-in module. Imaging was performed on *S. pombe* cells placed in sealed growth chambers containing 2% agarose yeast extract supplement medium.

Image analysis

*tts1*Δ cells coexpressing Rtn1-mCherry and GFP-fused Tts1 mutants or wild-type Tts1 were used to examine the specificity of Tts1 mutants in tubular ER localization (Figure 1B). Rtn1-mCherry–positive regions were considered as proxy for the tubular ER domains. Specificity was defined as the ratio of the average GFP fluorescence intensity in Rtn1-mCherry–marked regions to that in the rest of the cellular cortex territory. The values shown were normalized to the wild type.

The individual cell territory at the top plane was manually outlined based on the bright-field image. The top planes from *z*-stacks of Rtn1-mCherry were autothresholded in ImageJ (National Institutes of Health, Bethesda, MD). The fluorescent structures equal to or larger than 4 × 4 pixels (0.24 × 0.24 μm) were counted as tubular domains. The position and size of these fluorescent structures were measured by the Analyze Particles ImageJ built-in module within the cell territory.

ACKNOWLEDGMENTS

We are grateful to A. Vjestica for discussions and to P. Padmini and R. Jayadev for technical help. Special thanks go to Mary K. Morphew and Thomas H. Giddings from the Boulder Laboratory for 3D Electron Microscopy of Cells of the University of Colorado (Boulder, CO) for help with EM studies. Many thanks are also due to R. McIntosh, M. Sato. and M. Balasubramanian for sharing strains and reagents used in this work. This work was supported by the Singapore Millennium Foundation.

REFERENCES

Anderson DJ, Hetzer MW (2007). Nuclear envelope formation by chromatin-mediated reorganization of the endoplasmic reticulum. Nat Cell Biol 9, 1160–1166.

Anderson DJ, Hetzer MW (2008). Reshaping of the endoplasmic reticulum limits the rate for nuclear envelope formation. J Cell Biol 182, 911–924.

Antonin W, Mattaj IW (2005). Nuclear pore complexes: round the bend? Nat Cell Biol 7, 10–12.

Bae JA, Moon D, Yoon JH (2009). Nup211, the fission yeast homolog of Mlp1/Tpr, is involved in mRNA export. J Microbiol 47, 337–343.

Bahler J, Steever AB, Wheatley S, Wang Y, Pringle JR, Gould KL, McCollum D (1998). Role of polo kinase and Mid1p in determining the site of cell division in fission yeast. J Cell Biol 143, 1603–1616.

Bailey TL, Boden M, Buske FA, Frith M, Grant CE, Clementi L, Ren J, Li WW, Noble WS (2009). MEME SUITE: tools for motif discovery and searching. Nucleic Acids Res 37, W202–W208.

Belgareh N, Doye V (1997). Dynamics of nuclear pore distribution in nucleoporin mutant yeast cells. J Cell Biol 136, 747–759.

Bridge AJ, Morphew M, Bartlett R, Hagan IM (1998). The fission yeast SPB component Cut12 links bipolar spindle formation to mitotic control. Genes Dev 12, 927–942.

Casey AK, Dawson TR, Chen J, Friederichs JM, Jaspersen SL, Wente SR (2012). Integrity and function of the Saccharomyces cerevisiae spindle pole body depends on connections between the membrane proteins Ndc1, Rtn1, and Yop1. Genetics 192, 441–455.

Chadrin A, Hess B, San Roman M, Gatti X, Lombard B, Loew D, Barral Y, Palancade B, Doye V (2010). Pom33, a novel transmembrane nucleoporin required for proper nuclear pore complex distribution. J Cell Biol 189, 795–811.

Chernomordik LV, Kozlov MM (2003). Protein-lipid interplay in fusion and fission of biological membranes. Annu Rev Biochem 72, 175–207.

Chernomordik LV, Kozlov MM (2008). Mechanics of membrane fusion. Nat Struct Mol Biol 15, 675–683.

Contreras FX, Ernst AM, Wieland F, Brugger B (2011). Specificity of intramembrane protein-lipid interactions. Cold Spring Harb Perspect Biol 3, a004705.

Dawson TR, Lazarus MD, Hetzer MW, Wente SR (2009). ER membrane-bending proteins are necessary for de novo nuclear pore formation. J Cell Biol 184, 659–675.

Ding R, West RR, Morphew DM, Oakley BR, McIntosh JR (1997). The spindle pole body of Schizosaccharomyces pombe enters and leaves the nuclear envelope as the cell cycle proceeds. Mol Biol Cell 8, 1461–1479.

Fath S, Mancias JD, Bi X, Goldberg J (2007). Structure and organization of coat proteins in the COPII cage. Cell 129, 1325–1336.

Flory MR, Morphew M, Joseph JD, Means AR, Davis TN (2002). Pcp1p, an Spc110p-related calmodulin target at the centrosome of the fission yeast Schizosaccharomyces pombe. Cell Growth Differ 13, 47–58.

Fong CS, Sato M, Toda T (2010). Fission yeast Pcp1 links polo kinase-mediated mitotic entry to gamma-tubulin-dependent spindle formation. EMBO J 29, 120–130.

Fotin A, Cheng Y, Sliz P, Grigorieff N, Harrison SC, Kirchhausen T, Walz T (2004). Molecular model for a complete clathrin lattice from electron cryomicroscopy. Nature 432, 573–579.

Gautier R, Douguet D, Antonny B, Drin G (2008). HELIQUEST: a web server to screen sequences with specific alpha-helical properties. Bioinformatics 24, 2101–2102.

Giddings TH Jr, O'Toole ET, Morphew M, Mastronarde DN, McIntosh JR, Winey M (2001). Using rapid freeze and freeze-substitution for the preparation of yeast cells for electron microscopy and three-dimensional analysis. Methods Cell Biol 67, 27–42.

Gonzalez Y, Meerbrey K, Chong J, Torii Y, Padte NN, Sazer S (2009). Nuclear shape, growth and integrity in the closed mitosis of fission yeast depend

on the Ran-GTPase system, the spindle pole body and the endoplasmic reticulum. J Cell Sci 122, 2464–2472.
Gould KL (2004). Protocols for experimentation with Schizosaccharomyces pombe. Methods 33, 187–188.
Grallert A, Krapp A, Bagley S, Simanis V, Hagan IM (2004). Recruitment of NIMA kinase shows that maturation of the S. pombe spindle-pole body occurs over consecutive cell cycles and reveals a role for NIMA in modulating SIN activity. Genes Dev 18, 1007–1021.
Grigoriev I, Gouveia SM, van der Vaart B, Demmers J, Smyth JT, Honnappa S, Splinter D, Steinmetz MO, Putney JW Jr, Hoogenraad CC, *et al.* (2008). STIM1 is a MT-plus-end-tracking protein involved in remodeling of the ER. Curr Biol 18, 177–182.
Hetzer MW (2010). The nuclear envelope. Cold Spring Harb Perspect Biol 2, a000539.
Hodge CA, Choudhary V, Wolyniak MJ, Scarcelli JJ, Schneiter R, Cole CN (2010). Integral membrane proteins Brr6 and Apq12 link assembly of the nuclear pore complex to lipid homeostasis in the endoplasmic reticulum. J Cell Sci 123, 141–151.
Horio T, Uzawa S, Jung MK, Oakley BR, Tanaka K, Yanagida M (1991). The fission yeast gamma-tubulin is essential for mitosis and is localized at microtubule organizing centers. J Cell Sci 99, 693–700.
Hu J, Shibata Y, Voss C, Shemesh T, Li Z, Coughlin M, Kozlov MM, Rapoport TA, Prinz WA (2008). Membrane proteins of the endoplasmic reticulum induce high-curvature tubules. Science 319, 1247–1250.
Hu J, Shibata Y, Zhu PP, Voss C, Rismanchi N, Prinz WA, Rapoport TA, Blackstone C (2009). A class of dynamin-like GTPases involved in the generation of the tubular ER network. Cell 138, 549–561.
Jaspersen SL, Ghosh S (2012). Nuclear envelope insertion of spindle pole bodies and nuclear pore complexes. Nucleus 3, 226–236.
Lee C, Goldberg J (2010). Structure of coatomer cage proteins and the relationship among COPI, COPII, and clathrin vesicle coats. Cell 142, 123–132.
Lim HWG, Huber G, Torii Y, Hirata A, Miller J, Sazer S (2007). Vesicle-like biomechanics governs important aspects of nuclear geometry in fission yeast. PLoS One 2, e948.
Liu TY, Bian X, Sun S, Hu X, Klemm RW, Prinz WA, Rapoport TA, Hu J (2012). Lipid interaction of the C terminus and association of the transmembrane segments facilitate atlastin-mediated homotypic endoplasmic reticulum fusion. Proc Natl Acad Sci USA 109, E2146–E2154.
McMahon HT, Gallop JL (2005). Membrane curvature and mechanisms of dynamic cell membrane remodelling. Nature 438, 590–596.
Moritz M, Agard DA (2001). Gamma-tubulin complexes and microtubule nucleation. Curr Opin Struct Biol 11, 174–181.
Ohkura H, Hagan IM, Glover DM (1995). The conserved Schizosaccharomyces pombe kinase plo1, required to form a bipolar spindle, the actin ring, and septum, can drive septum formation in G1 and G2 cells. Genes Dev 9, 1059–1073.
Orso G, Pendin D, Liu S, Tosetto J, Moss TJ, Faust JE, Micaroni M, Egorova A, Martinuzzi A, McNew JA, *et al.* (2009). Homotypic fusion of ER membranes requires the dynamin-like GTPase atlastin. Nature 460, 978–983.
Palsdottir H, Hunte C (2004). Lipids in membrane protein structures. Biochim Biophys Acta 1666, 2–18.
Petersen B, Petersen TN, Andersen P, Nielsen M, Lundegaard C (2009). A generic method for assignment of reliability scores applied to solvent accessibility predictions. BMC Struct Biol 9, 51.
Rao Y, Haucke V (2011). Membrane shaping by the Bin/amphiphysin/Rvs (BAR) domain protein superfamily. Cell Mol Life Sci 68, 3983–3993.
Roux A, Cuvelier D, Nassoy P, Prost J, Bassereau P, Goud B (2005). Role of curvature and phase transition in lipid sorting and fission of membrane tubules. EMBO J 24, 1537–1545.
Sheetz MP (2001). Cell control by membrane-cytoskeleton adhesion. Nat Rev Mol Cell Biol 2, 392–396.
Shibata Y, Hu J, Kozlov MM, Rapoport TA (2009). Mechanisms shaping the membranes of cellular organelles. Annu Rev Cell Dev Biol 25, 329–354.
Shibata Y, Shemesh T, Prinz WA, Palazzo AF, Kozlov MM, Rapoport TA (2010). Mechanisms determining the morphology of the peripheral ER. Cell 143, 774–788.
Shibata Y, Voss C, Rist JM, Hu J, Rapoport TA, Prinz WA, Voeltz GK (2008). The reticulon and DP1/Yop1p proteins form immobile oligomers in the tubular endoplasmic reticulum. J Biol Chem 283, 18892–18904.
Sparkes I, Tolley N, Aller I, Svozil J, Osterrieder A, Botchway S, Mueller C, Frigerio L, Hawes C (2010). Five Arabidopsis reticulon isoforms share endoplasmic reticulum location, topology, and membrane-shaping properties. Plant Cell 22, 1333–1343.
Stagg SM, LaPointe P, Razvi A, Gurkan C, Potter CS, Carragher B, Balch WE (2008). Structural basis for cargo regulation of COPII coat assembly. Cell 134, 474–484.
Strambio-de-Castillia C, Blobel G, Rout MP (1999). Proteins connecting the nuclear pore complex with the nuclear interior. J Cell Biol 144, 839–855.
Tallada VA, Tanaka K, Yanagida M, Hagan IM (2009). The S. pombe mitotic regulator Cut12 promotes spindle pole body activation and integration into the nuclear envelope. J Cell Biol 185, 875–888.
Tamm T, Grallert A, Grossman EP, Alvarez-Tabares I, Stevens FE, Hagan IM (2011). Brr6 drives the Schizosaccharomyces pombe spindle pole body nuclear envelope insertion/extrusion cycle. J Cell Biol 195, 467–484.
Tusnady GE, Simon I (2001). The HMMTOP transmembrane topology prediction server. Bioinformatics 17, 849–850.
Vardy L, Toda T (2000). The fission yeast gamma-tubulin complex is required in G(1) phase and is a component of the spindle assembly checkpoint. EMBO J 19, 6098–6111.
Voeltz GK, Prinz WA, Shibata Y, Rist JM, Rapoport TA (2006). A class of membrane proteins shaping the tubular endoplasmic reticulum. Cell 124, 573–586.
Voeltz GK, Rolls MM, Rapoport TA (2002). Structural organization of the endoplasmic reticulum. EMBO Rep 3, 944–950.
Wagner W, Brenowitz SD, Hammer JA 3rd (2011). Myosin-Va transports the endoplasmic reticulum into the dendritic spines of Purkinje neurons. Nat Cell Biol 13, 40–48.
West RR, Vaisberg EV, Ding R, Nurse P, McIntosh JR (1998). cut11(+): A gene required for cell cycle-dependent spindle pole body anchoring in the nuclear envelope and bipolar spindle formation in Schizosaccharomyces pombe. Mol Biol Cell 9, 2839–2855.
Witkin KL, Friederichs JM, Cohen-Fix O, Jaspersen SL (2010). Changes in the nuclear envelope environment affect spindle pole body duplication in Saccharomyces cerevisiae. Genetics 186, 867–883.
Yam C, Gu Y, Oliferenko S (2013). Partitioning and remodeling of the Schizosaccharomyces japonicus mitotic nucleus require chromosome tethers. Curr Biol 23, 2303–2310.
Yam C, He Y, Zhang D, Chiam KH, Oliferenko S (2011). Divergent strategies for controlling the nuclear membrane satisfy geometric constraints during nuclear division. Curr Biol 21, 1314–1319.
Zhang D, Oliferenko S (2013). Remodeling the nuclear membrane during closed mitosis. Curr Opin Cell Biol 25, 142–148.
Zhang D, Vjestica A, Oliferenko S (2010). The cortical ER network limits the permissive zone for actomyosin ring assembly. Curr Biol 20, 1029–1034.
Zhang D, Vjestica A, Oliferenko S (2012). Plasma membrane tethering of the cortical ER necessitates its finely reticulated architecture. Curr Biol 22, 2048–2052.
Zheng Y, Wong ML, Alberts B, Mitchison T (1995). Nucleation of microtubule assembly by a gamma-tubulin-containing ring complex. Nature 378, 578–583.